Activation Volumes for Solid-Solid Transformations in Nanocrystals

Keren Jacobs, David Zaziski, Erik C. Scher, Amy B. Herhold,* A. Paul Alivisatos†

The transition between four- and six-coordinate structures in CdSe nanocrystals displays simple transition kinetics as compared with the extended solid, and we determined activation volumes from the pressure dependence of the relaxation times. Our measurements indicate that the transformation takes place by a nucleation mechanism and place strong constraints on the type of microscopic motions that lead to the transformation. The type of analysis presented here is difficult for extended solids, which transform by complicated kinetics and involve ill-defined domain volumes. Solids patterned on the nanoscale may prove to be powerful models for the general study of structural transitions in small systems, as well as in extended solids.

An understanding of first-order structural transitions is relevant to many research areas, including the study of solids at high pressures and the engineering of materials with enhanced mechanical properties. For example, solid-solid transitions in silicates in the Earth's mantle are thought to play a vital role in plate tectonics and earthquakes (*1*, *2*). In geological applications, models of structural-transition kinetics must simulate rock formation taking place over millions of years (*3*). Structural transitions are also used in the production of steel during heat treatment of iron-carbide alloys and in producing ceramic materials with exceptionally high fracture toughness, such as partially stabilized zirconia (*4*). Despite their importance for materials and planetary science, the microscopic mechanisms of solid-solid phase transitions are difficult to study for several reasons. The kinetics of a transformation in an extended solid is highly inhomogeneous, with different processes occurring in parallel in different parts of the sample. Transformations in extended solids are dominated by growth mechanisms and have inherently irreproducible transition cycles because new defects are generated during the course of the transition.

The study of phase transitions can be greatly simplified in nanocrystal systems because small crystals can behave as single structural domains and reproducibly cycle through multiple transformations (*5*). For this reason, theoretical investigations into structural transformations in nanocrystals are now being performed by several groups (*6*–*8*). We show that it is experimentally possible to measure one of the fundamental properties of a chemical reaction, the activation volume, for a solid-solid transition in nanocrystals. By taking advantage of the simple kinetics in a nanocrystal system, we obtain insight into the mechanisms and microscopic processes of structural phase transitions.

CdSe nanocrystals can be used as model systems for structural studies (*9*). The nanocrystals consist of hundreds to thousands of covalently bonded atoms, synthesized as nearly defect-free crystals with narrow size distribution and controlled shape (*10*). At low pressures, the atoms are tetrahedrally bonded and form a hexagonal network of stacked sheets with wurtzite and zinc blende stacking sequences. At high pressures, the nanocrystals contract by 18% as they transform to a denser, six-coordinate rock-salt structure. Transformation cycles between the structures are not observed at the thermodynamic transition pressure, where the free energies of the phases are equal. Instead, an energetic barrier along the transition pathway hinders the transition and results in a hysteresis loop, which reflects the time needed for the system to relax to the equilibrium configuration. The hysteresis of the CdSe nanocrystal transition is sufficiently extensive for the study of structural phase transitions despite their finite extent. In small systems, smearing of the thermodynamic transition can arise from thermal fluctuations between the structures (*11*). In the smallest nanocrystals under study here (25 Å in diameter, ~300 atoms), the total volume change during the transition is ~1500 Å^3. Because the differential of free energy with respect to pressure is volume, we estimate that the corresponding thermal fluctuations smear the nanocrystal transition by less than 0.1 GPa at 500 K. This smearing is insignificant compared with the kinetics-induced hysteresis width of ~6 GPa and implies that the transition is observed "far" from equilibrium conditions even in nanocrystals.

The microscopic structure of large nanocrystals before and after a transition cycle is shown in Fig. 1 (*12*–*15*). Well-defined crystal volumes and structures are involved in the nanocrystal transformation, because the tetrahedral bonding between the Cd and Se atoms remains uninterrupted even after pressure cycling. The transition was monitored through changes in the visible absorption of the sample after an abrupt increase or decrease in the pressure (*16*). Extensive kinetics measurements of transformation times were made as a function of pressure and temperature in nanocrystals between 25 and 35 Å in diameter. In Fig. 2, typical relaxation times are shown for 25 Å diameter nanocrystals for several pressures. The time dependence of the transition is fit with a simple exponential decay in both transition directions, from which the rate constants are extracted.

The observation of simple transition kinetics even after multiple transitions is evidence of the single-domain behavior in nanocrystals. The activation energy (enthalpic barrier) was determined from the temperature dependence of the rate constants as 0.9 and 0.2 ± 0.1 eV per nanocrystal (21 and 4.6 kcal/mol of nanocrystals) for 25 Å diameter nanocrystals in the forward and reverse directions, respectively. The activation volume ($\Delta V^{\ddagger}$), or the volume change between the transition state and reactant, is determined from the pressure dependence of the rate constants (Fig. 3A), with the following expression from transition state theory:

$$\left(\frac{\partial \ln(k)}{\partial P}\right)_T = \frac{-\Delta V^{\ddagger}}{k_B T} \qquad (1)$$

where $k_B T$ is thermal energy (Boltzmann's constant k_B times temperature T), P is pressure, and k is the rate constant (*17*). The activation volumes are −17 and +65 Å^3 for 25 Å diameter nanocrystals in the forward and reverse transition directions, respectively.

The smaller volume deformation during the forward transformation indicates that the transition state more closely resembles the four-coordinate structure than the six-coordinate structure. A transition state that is not precisely midway between the two stable minima is reasonable in transformations between phases with differing volumes. This asymmetry has profound consequences for the hysteresis loop, which is observed to narrow by 40% as the relaxation time increases from 15 s (ln k = −3) to 20 min (ln k = −7.5) at a constant temperature of 463 K (Fig. 3A). Using a linear extrapolation, we estimate that the hysteresis will ultimately collapse about a thermodynamic transition pressure of 2.3 GPa with a relaxation time of

---

Department of Chemistry, University of California, Berkeley, Berkeley, CA 94720, USA, and Materials Science Division, Lawrence Berkeley National Laboratory, 1 Cyclotron Road, Berkeley, CA 94720, USA.

*Present address: Corporate Strategic Research, Exxon Mobil Research and Engineering Company, Route 22 East, Annandale, NJ 08801, USA.

†To whom correspondence should be addressed. E-mail: alivis@uclink4.berkeley.edu

>10 years at room temperature. By default, thermodynamic transition pressures for structural transformations are frequently taken as the center of the hysteresis loop (*3*, *18*). However, here this pressure is observed to be markedly lower than the hysteresis center and is the direct result of different activation volumes in the two transition directions. This result is consistent with the observation of different activation energies in the two transition directions, indicated by the greater sensitivity of the forward transition to temperature (Fig. 3B).

Additional information regarding the transition state is obtained from the opposite signs of the activation volumes, which imply that the transition state must be intermediate in volume between that of the two structures (Fig. 3A schematic), unlike a system that expands in both directions to accommodate the atomic rearrangements. For example, the graphite-diamond transition in carbon has a fluidlike transition state that hinders the transition with increasing pressure (*3*, *19*) and should produce positive activation volumes in both transition directions. However, the case of an intermediate transition-state volume observed here is probably more common for transitions that exhibit conventional hysteresis loops (the forward transition is facilitated with increasing pressure). It is inherently implied in classical nucleation models for structural transitions (*20*), in which the transition state is an average volume of both structures. In such models, the activation volume is proportional to the critical nucleus size because it is equivalent to the volume change that accompanies its formation. Nucleation theory also predicts that the critical nucleus size should vary with pressure, but is largest at the thermodynamic transition pressure. This premise is consistent with the experimental activation volumes, which should increase in magnitude "near" the thermodynamic pressure in order for the forward and reverse activation volumes to add up suitably to the 18% total volume change across the transition.

The microscopic mechanism from which the hysteresis originates is constrained by the small magnitude of the activation volume of ~0.2% in comparison with the 18% total volume change. The simplest model is a coherent deformation mechanism involving coordinated motion throughout the crystal lattice (*21*). However, this model is inconsistent with the activation volume, because 0.2% distributed throughout the nanocrystal is even smaller than the volume change caused by

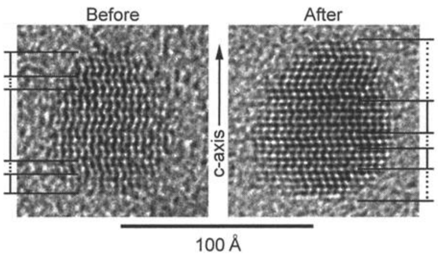

Fig. 1. High-resolution transmission electron micrograph of representative CdSe nanocrystals in the four-coordinate structure before and after pressure cycling. The arrow indicates the unique *c* axis, along which (001) layers are stacked. Two possible stacking sequences, ABAB- and ABCABC-, yield the nearly isoenergetic wurtzite (hexagonally close-packed) and zinc blende (face-centered cubic) structures within the nanocrystal. Wurtzite stacking is indicated with solid lines, zinc blende stacking with dashed lines. After pressure cycling, the nominally spherical shape recovers and the nanocrystal has an increased fraction of zinc blende layers, which is consistent with previous interpretations of x-ray diffraction measurements (*5*). The stacking faults are a particularly simple type of grain boundary, but do not interrupt the connectivity of the atoms in the nanocrystal. The (001) layers shown here are involved in the shearing motion of the sliding planes mechanism described in the text.

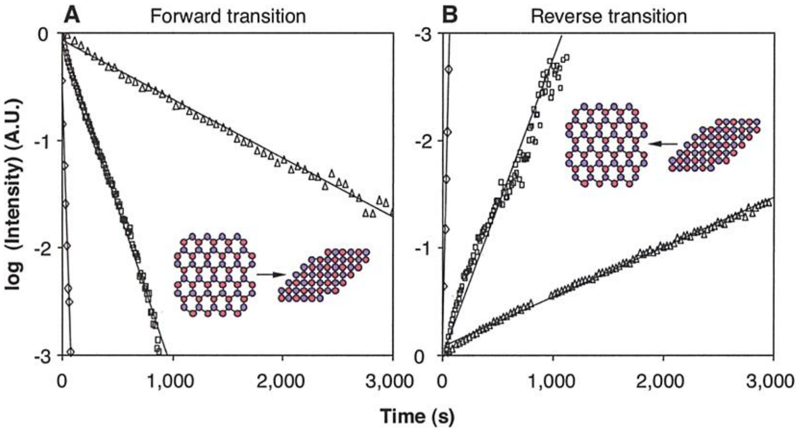

Fig. 2. Time dependence of the transformation in 25 Å CdSe crystals at 463 K at different pressures. (**A**) The forward transition at (△) 5.2 GPa, (□) 5.7 GPa, and (◇) 6.9 GPa. (**B**) The reverse transition at (◇) 0.7 GPa, (□) 1.0 GPa, and (△) 1.2 GPa. (1 GPa ≅ 10,000 atm). The abscissa is the intensity of the four-coordinate electronic absorption feature (*16*). Fits are single-exponential decays. Rate constants were obtained from the slope of the fitted lines and are equivalent to relaxation times (= ln 2/k) in the forward transition of: (△) 21 min, (□) 3.6 min, and (◇) 20 s. In the reverse transition: (◇) 16 s, (□) 3.8 min, and (△) 24 min. Each crystal in the ensemble transforms instantaneously relative to the experiment time such that the relaxation is a measure of the average time required to overcome the kinetic barrier. Once a nanocrystal transforms to the stable structure, it is statistically unlikely that it will fluctuate back unless the pressure is changed accordingly, because the transition is measured "far" from equilibrium. The shape changes shown in the schematic were determined from simulations of x-ray diffraction patterns and is consistent with the sliding planes mechanism (*5*).

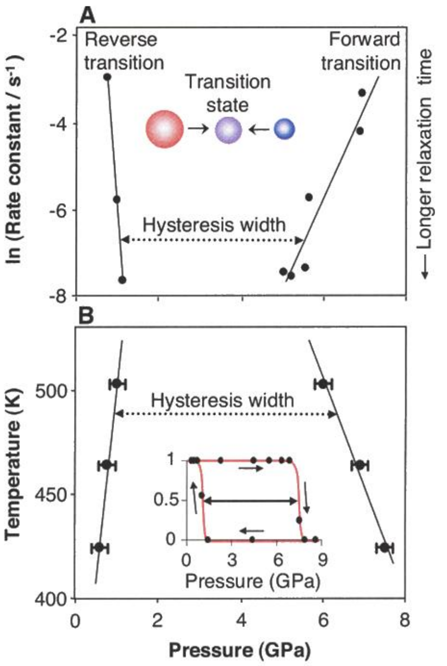

Fig. 3. Hysteresis loop dependence on (**A**) relaxation time and (**B**) temperature for the transformation in 25 Å diameter CdSe nanocrystals. (A) The rate constants are determined from time-dependent decays at 463 K, such as those shown in Fig. 2. Activation volumes determined from the slopes with Eq. 1 are −17 Å^3 and +65 Å^3 in the forward and reverse transitions, respectively. The activation volumes are assumed to be constant over the pressure ranges under study to simplify the analysis. Even small, microscopic-volume deformations during the transition change the rate constant by several orders of magnitude in only a fraction of a GPa change in pressure. (B) The temperature data are compiled from measurements of the rate constant for ln (k) = −3.5 at the given temperatures. The hysteresis loop systematically narrows with increasing temperature, as expected for an activated process. (Inset) A sample hysteresis loop measured for 35 Å nanocrystals with the hysteresis width indicated. The loop starts at low pressure and proceeds in the direction of the arrows, as the normalized ratio of sample transformed is monitored.

thermal vibrations of the crystal lattice. A nucleation mechanism involving just part of the crystal is more plausible because it requires only a modest structural deformation. A spherically shaped nucleus is excluded because the activation volume would correspond to a nucleus smaller than the size of a unit cell. In addition, this case is inconsistent with the observation of an increasing activation-volume magnitude from 17 to 34 and 124 Å^3 in the forward direction for 25, 30, and 35 Å diameter nanocrystals, respectively. The data instead strongly support directionally dependent nucleation such as a sliding planes mechanism, involving a shearing motion of the (001) crystal planes (shown in Fig. 1) relative to one another (*5*). This explains the variation in the stacking sequence along the *c* axis observed before and after the transition in Fig. 1 (*22*), because the transition is directionally dependent and not sensitive to the stacking along this axis. This type of mechanism is established in the study of martensitic transitions (*23*) and is consistent with the increasing activation volume with size.

Previous studies showing increasing activation energies with size (*24*, *25*) are now understood as arising from additional bonds that must break as the planes in larger particles slide. The measured activation energies are in marked agreement with our estimates of the energy necessary to shear the (001) plane, as determined with the stacking fault energy of 14 meV per atom reported by Maeda and co-workers (*26*). For example, the activation energy of 0.9 eV in 25 Å nanocrystals (~50 atoms per plane) compares well with an estimate of 0.7 eV based on the transformation model. Although martensitic transitions are generally considered athermal, the shearing appears to be activated in this nanocrystal transition, perhaps because the role of defects has been eliminated.

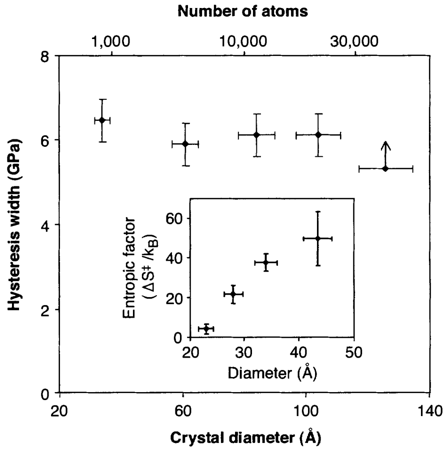

Fig. 4. Hysteresis width versus nanocrystal size at room temperature and a relaxation time of ~3 min. The width for the largest sample is a lower limit because the 126 Å diameter nanocrystals remain trapped in the high-pressure rock-salt structure as the pressure is released (*40*). In the inset, $\Delta S^\ddagger$ is the entropic barrier and k_B is Boltzmann's constant. The entropic factor was determined from intercepts of Arrhenius plots (*29*).

It was previously presumed that the nanocrystal was small enough to transform between solids in a coherent deformation process and that the critical nucleus was larger than several nanometers in diameter (*25*). The observation of a local nucleation mechanism in nanocrystals modifies this guess for a critical nucleus size, and the directional dependence of the mechanism suggests an "easy axis" for the transition and a critical nucleus in the extended solid that is not spherically shaped. In much larger crystals, nucleation initiated at defects may come into play, whereas much smaller crystals may more closely resemble molecular isomerizations. If this lower limit occurs at a definable crystal size, the structures would flip back and forth at thermal equilibrium with minimal hysteresis. Structural fluctuations of this type are thought to occur in some gas-phase inorganic cluster species (*27*).

To further understand the transition mechanism, we measured the size dependence of the hysteresis width at room temperature in nanocrystal sizes up to 130 Å in diameter, a 30-fold volume increase compared with previous studies (*9*). The nearly constant hysteresis width of ~6 GPa over this size range implies that the corresponding free-energy barrier responsible for the hysteresis is insensitive to nanocrystal size (Fig. 4). The increasing entropic factor as a function of size (Fig. 4 inset) accounts for the observed behavior because it offsets the increasing activation energy with size (*24*). This is uncharacteristic of a coherent deformation mechanism, for which the hysteresis width should strongly broaden with size without increasing entropic factors. Instead, the trends with size are indicative of a nucleation mechanism with multiple sites from which the transition can initiate. In the proposed transformation model, this corresponds to greater probability of nucleation in nanocrystals with larger numbers of planes because only one nucleation event occurs per nanocrystal transformation. If high enough temperatures were experimentally feasible in this system (*28*, *29*), the hysteresis should ultimately narrow with increasing crystal size owing to the greater influence of the entropic factor. Unlike the alternative models, the directionally dependent nucleation model is consistent with the entire set of observations.

A useful comparison for solid-solid transformations in nanocrystals is with the well-studied case of magnetic transitions in nanocrystals used in everyday storage media. The transitions are analogous in thermodynamics and statistical mechanics with the appropriate substitution of variables (*30*). Although both transitions can behave as single domains in nanocrystal systems, differences between the transitions are apparent with these experiments. The asymmetry of the hysteresis loop in the structural transition is in contrast to magnetic transitions, which have symmetric hysteresis because the two phases are indistinguishable in the absence of a magnetic field. Furthermore, the CdSe nanocrystal is found to transform between solids by local deformation followed by rapid growth, whereas magnetic transitions in similar crystal sizes involve coherent rotation of the nanocrystal "super-spin" described by the well-known Néel-Brown model (*31*, *32*). The onset of nucleation mechanisms in magnetism does not occur until crystal sizes are greater than 300 Å (*33*). Interestingly, in the size range of 300 to 2000 Å, magnetic transitions also exhibit nearly size-independent hysteresis widths (*34*, *35*). This rescaling of crystal size is related to the relative energies involved in the transformation processes. The area of the hysteresis loop representing the irreversible work in a transition cycle is equivalent to more than 770,000 times the thermal energy in the CdSe structural transition, but to only 125 times in Co-Fe alloy magnetic nanocrystals in 100 Å nanocrystals (*36*–*39*). Thus, the irreversible energy released in a cycle is three to four orders of magnitude larger in the structural transition. Larger energy barriers are involved in reorganizing bonds than in reversing the magnetization, such that the structural transition in nanocrystals cannot physically involve the entire crystal lattice. Significant insight into the microscopic processes of many other solid-solid phase transitions of importance in materials science and geophysics may emerge through future studies of nanocrystals.

References and Notes

1. S. H. Kirby, W. B. Durham, L. A. Stern, *Science* **252**, 216 (1991).
2. A. Putnis, *Introduction to Mineral Sciences* (Cambridge Univ. Press, Cambridge, 1992).
3. N. V. C. Shekar, K. G. Rajan, *Bull. Mater. Sci.* **24**, 1 (2001).
4. W. F. Smith, *Principles of Materials Science and Engineering* (McGraw-Hill, New York, ed. 3, 1996).
5. J. N. Wickham, A. B. Herhold, A. P. Alivisatos, *Phys. Rev. Lett.* **84**, 4515 (2000).
6. C. Molteni, R. Martonak, M. Parrinello, *J. Chem. Phys.* **114**, 5358 (2001).
7. S. Kodiyalam *et al.*, *Phys. Rev. Lett.* **86**, 55 (2001).
8. S. Leoni, R. Nesper, *Acta. Crystallogr. A* **56**, 383 (2000).
9. S. H. Tolbert, A. P. Alivisatos, *J. Chem. Phys.* **102**, 4642 (1995).
10. X. Peng *et al.*, *Nature* **404**, 59 (2000).
11. T. L. Hill, *Thermodynamics of Small Systems* (Dover, New York, 1963).
12. Spherically shaped nanocrystals between 25 and 130 Å in diameter (σ = 5 to 10%) were synthesized as described (*13*, *14*). The samples were coated with an organic ligand (tri-*n*-octylphosphine oxide) and dissolved in ethylcyclohexane to disperse the particles and act as the pressure-transmitting medium. Pres-

sures between 0 and 10 GPa were applied with a diamond anvil cell (DAC) and were measured with standard ruby fluorescence techniques to ±0.2 GPa (*15*).

13. C. B. Murray, D. J. Norris, M. G. Bawendi, *J. Am. Chem. Soc.* **115**, 8706 (1993).
14. X. G. Peng, J. Wickham, A. P. Alivisatos, *J. Am. Chem. Soc.* **120**, 5343 (1998).
15. For a review of ruby measurements, see J. D. Barnett, S. Block, G. J. Piermari, *Rev. Sci. Instrum.* **44**, 1 (1973).
16. The four-coordinate structure is a direct band-gap semiconductor with an electronic absorbance peak in the visible spectrum, whereas the six-coordinate structure is an indirect band-gap semiconductor and has a featureless spectrum [see also (*25*)]. Light from a tungsten-halogen source was sent through a sample loaded in the DAC. The transmitted light was directed into a spectrometer and detected with a liquid N_2–cooled charge-coupled device camera. Static temperature control to 510 K was achieved by placing the cell in a resistively heated ceramic oven and was measured with a thermocouple in contact with the diamond. Remote control of the pressure in the DAC by a computer-controlled stepper motor made it possible to measure relatively fast transition times on the order of seconds.
17. M. G. Evans, M. Polanyi, *Trans. Faraday Soc.* **1935** (1935).
18. X. Y. Li, R. Jeanloz, *Phys. Rev. B* **36**, 474 (1987).
19. F. P. Bundy, *Proc. K. Ned. Akad. Wet. Ser. B Phys. Sci.* **72**, 302 (1969).
20. J. W. Christian, *The Theory of Transformations in Metals and Alloys*, Part 1, Equilibrium and General Kinetic Theory (Pergamon, Oxford, New York, 1965).
21. L. E. Brus, J. A. W. Harkless, F. H. Stillinger, *J. Am. Chem. Soc.* **118**, 4834 (1996).
22. J. Osugi, K. Shimizu, T. Nakamura, A. Onodera, *Rev. Phys. Chem. Jpn.* **36**, 59 (1966).
23. D. A. Porter, K. E. Easterling, *Phase Transformations in Metals and Alloys* (Chapman and Hall, London, ed. 2, 1992).
24. Increasing activation energies of 0.5, 1.2, 1.7, and 2.4 eV/nanocrystal were reported for CdSe nanocrystal diameters of 20, 27, 34, and 43 Å, respectively, in the forward transition; see (*25*).
25. C. C. Chen, A. B. Herhold, C. S. Johnson, A. P. Alivisatos, *Science* **276**, 398 (1997).
26. S. Takeuchi, K. Suzuki, K. Maeda, H. Iwanaga, *Philos. Mag. A.* **50**, 171 (1984).
27. R. S. Berry, B. M. Smirnov, *J. Chem. Phys.* **113**, 728 (2000).
28. Above a temperature limit of 575 K, interparticle diffusion can occur and the nanocrystals are no longer isolated and distinct particles; see (*29*).
29. A. B. Herhold, thesis, University of California, Berkeley (1997).
30. L. D. Landau, E. Lifshitz, *Statistical physics*, J. B. Sykes, M. J. Kearsley, Eds. (Pergamon, New York, 1980).
31. L. Néel, *Compt. Rend. Acad. Sci. Paris* **228**, 664 (1949).
32. W. F. Brown, *Ann. NY Acad. Sci.* **147**, 461 (1969).
33. H. L. Richards, M. Kolesik, P.-A. Lindgard, *Phys. Rev. B* **55**, 11521 (1997).
34. M. J. O'Shea, H. Jiang, P. Perera, H. H. Hamdeh, *J. Appl. Phys.* **87**, 6137 (2000).
35. T. Chang, J.-G. Zhu, J. H. Judy, *J. Appl. Phys.* **73**, 6716 (1993).
36. We used magnetization of 0.15 A·m^2 per gram in 100 Å Fe-Co crystals and the permeability in free space for hysteresis loops taken at 76 K; see (*37*).
37. F. E. Luborsky, T. O. Paine, *J. Appl. Phys.* **31**, S68-S70 (1960).
38. The large structural hysteresis area is consistent with the smearing calculation, indicating that experimental temperatures are small relative to the thermal energy of the structural hysteresis. The energy disparity between the transitions is related to the fact that superparamagnetism (free-energy barrier is on the order of thermal energy) often occurs in magnetic nanocrystals, while the structural analog has yet to be observed in nanocrystals. The disparity is also quantitatively consistent with the 10-year relaxation time at the thermodynamic pressure in 25 Å CdSe nanocrystals, which occurs in a magnetic transition in nanocrystals over 200 Å in diameter; see (*39*).
39. H. J. Richter, *J. Phys. D Appl. Phys.* **32**, R147 (1999).
40. K. Jacobs *et al.*, in preparation.
41. We thank J. Wickham, R. Jeanloz, and G. Inger for helpful discussions and E. Granlund and H. Gretch for machining work on the DAC. This work was supported by the director, Office of Energy Research, Office of Science, Division of Materials Sciences, of the U. S. Department of Energy, and the Air Force Office of Scientific Research, Air Force Material Command, U.S. Air Force. We used the facilities of the National Center for Electron Microscopy for the electron microscope images.

19 June 2001; accepted 9 August 2001

Antibody Catalysis of the Oxidation of Water

Paul Wentworth Jr.,[1] Lyn H. Jones,[1] Anita D. Wentworth,[1]
Xueyong Zhu,[1] Nicholas A. Larsen,[1] Ian A. Wilson,[1] Xin Xu,[2]
William A. Goddard III,[2] Kim D. Janda,[1] Albert Eschenmoser,[1,3]
Richard A. Lerner[1]

Recently we reported that antibodies can generate hydrogen peroxide (H_2O_2) from singlet molecular oxygen ($^1O_2^*$). We now show that this process is catalytic, and we identify the electron source for a quasi-unlimited generation of H_2O_2. Antibodies produce up to 500 mole equivalents of H_2O_2 from $^1O_2^*$, without a reduction in rate, and we have excluded metals or Cl^- as the electron source. On the basis of isotope incorporation experiments and kinetic data, we propose that antibodies use H_2O as an electron source, facilitating its addition to $^1O_2^*$ to form H_2O_3 as the first intermediate in a reaction cascade that eventually leads to H_2O_2. X-ray crystallographic studies with xenon point to putative conserved oxygen binding sites within the antibody fold where this chemistry could be initiated. Our findings suggest a protective function of immunoglobulins against $^1O_2^*$ and raise the question of whether the need to detoxify $^1O_2^*$ has played a decisive role in the evolution of the immunoglobulin fold.

Antibodies, regardless of source or antigenic specificity, generate H_2O_2 from $^1O_2^*$, thereby potentially aligning recognition and killing within the same molecule (*1*). Given the potential chemical and biological importance of this observation, the mechanistic basis of this process and its structural location within the antibody have been investigated. Together these studies reveal that antibodies, in contrast to other proteins, may catalyze an unprecedented set of chemical reactions between water and $^1O_2^*$.

Long-term ultraviolet (UV) irradiation studies reveal that antibody-mediated H_2O_2 production is much more efficient than for non-immunoglobulin proteins (Fig. 1A). Typically antibodies exhibit linearity in H_2O_2 formation for up to 40 mole equivalents of H_2O_2 before the rate begins to decline asymptotically (Fig. 1B). Non-immunoglobulin proteins display a short burst of H_2O_2 production followed by quenching as photo-oxidation occurs (Fig. 1A). Also, antibodies can resume photoproduction of H_2O_2 at the same initial rate if H_2O_2 is removed by catalase (Fig. 1C). Thus, H_2O_2 reversibly inhibits its own formation. The apparent median inhibitory concentration (IC_{50}) was estimated as 225 μM (Fig. 1E). Antibody-mediated photoproduction of H_2O_2 can also be saturated with molecular oxygen (apparent Michaelis-Menten constant for oxygen = 187 μM) (*1*), which, when allied with the H_2O_2 inhibition aspect, suggests a binding site process.

Even after 10 cycles of UV irradiation followed by addition and removal of catalase (which generates ~500 mole equivalents of H_2O_2), only a slight reduction (5%) is seen in the initial rate. Beside antibodies, the only other protein that we have found thus far to generate H_2O_2 catalytically is the αβ T cell receptor (αβTCR) (Fig. 1D), which shares a similar arrangement of its immunoglobulin fold domains with antibodies (*2*). However, possession of this structural motif does not necessarily confer an H_2O_2-generating ability on proteins; β_2-microglobulin, although a member of the immunoglobulin superfamily (*3*), does not generate H_2O_2.

The antibody structure is remarkably inert to the oxidizing effects of H_2O_2. SDS–polyacrylamide gel electrophoresis of antibody samples after UV irradiation under standard conditions for 8 hours revealed no significant fragmenta-

---

[1] Departments of Chemistry and Molecular Biology and Skaggs Institute for Chemical Biology, Scripps Research Institute, 10550 North Torrey Pines Road, La Jolla, CA 92037, USA. [2] Materials and Process Simulation Center, Division of Chemistry and Chemical Engineering (MC 139-74), California Institute of Technology, Pasadena, CA 91125, USA. [3] Laboratorium für Organische Chemie, Eidgenössische Technische Hochschule (ETH) Zürich, Universitätstrasse 16, CH-8092 Zürich, Switzerland.